Development of the Specular Echoes Estimator to predict relevant modes for Total Focusing Method imaging

Kombossé Sy, Philippe Brédif, Ekaterina Iakovleva, Olivier Roy, Dominique Lesselier

Development of the specular echoes estimator to predict relevant modes for Total Focusing Method imaging

Kombossé Sy[a,b,c,*], Philippe Brédif[a], Ekaterina Iakovleva[a], Olivier Roy[b], Dominique Lesselier[c]

[a]CEA List, Centre de Saclay, Bâtiment Digiteo 565, 91191 Gif-sur-Yvette, France
[b]M2M, 1, rue de Terre Neuve, 91940 Les Ulis, France
[c]Laboratoire des Signaux et Systèmes, UMR8506 (CNRS-CentraleSupélec-Univ. Paris-Sud), Université Paris-Saclay, 91192 Gif-sur-Yvette, France

Total Focusing Method imaging is an ultrasonic testing method which has emerged in recent years as an alternative to standard phased array inspection methods in non-destructive testing, due to its high resolution and the realistic images of defects that it provides. In the case of crack-like defects, it provides images where the profile and the tips of the defects are reconstructed. TFM imaging is a procedure which yields the spatial position of the reflectors from which the main transient signals observed in the data are originated from. Thereby, diffraction echoes are located at the tips of the defect, and specular echoes appear along the profile of the defect. This signature allows the characterization of the planar nature of the defect. However, a correct reconstruction requires the use of the relevant ultrasonic path to produce the echoes wanted among a large number of possible paths between the array transducer and the reflector. In this paper, we have developed a method based on physical considerations, for predicting relevant paths. The tool is applied in several inspection configurations involving notches nearby welds. Validation is achieved from a variety of synthetic and experimental results.

1. Introduction

Defect characterization is essential in non destructive testing: the defect nature allows for predicting its potential evolution. Volumetric defects, such as porosity and inclusions, are generally not dangerous for the material, while plane defects, such as cracks, can lead to critical failures. For both kinds of defects standard conventional and phased array methods provide very close signatures, and it requires an analysis by a specialist operator to distinguish them.

The Total Focusing Method (TFM) [1–5] exhibits a main advantage for defect characterization by providing different signatures for different kinds of defects. TFM imaging focuses temporal signals at the spatial position of the reflectors. Thereby, in the case of crack like defects, diffraction echoes are located at the defect extremities, and specular echoes along the defect profile. The latter allows conclusions to be drawn about the nature of the defect.

Due to their unidirectional nature (Snell-Descartes' law), specular echoes are more sensitive to defect orientation than omnidirectional diffraction echoes. So, it is necessary to determine the relevant path producing the echoes wanted among a large number of possible paths between the array transducer and the reflector, due to direct paths, reflection on the back wall and wave mode conversion. Indeed, not all these paths will produce a true defect profile and in addition artefacts may occur, complicating image interpretation.

The present work investigates new methods to automatically determine relevant paths (also called reconstruction modes) depending on the known parameters of the inspection.

This paper is organized as follows: we recall the principle of TFM imaging, and we point out the echoes resulting from various modes of reconstruction. Then we show how to exploit diffraction and specular echoes for defect characterization. Thereafter, we propose a new tool, called Specular Echoes Estimator (SEE), which we have developed to predict relevant modes. Finally, experimental and modelling results are used to demonstrate the capabilities of this tool.

2. Principle of TFM imaging

TFM imaging is a method of focusing at any point of a defined region of interest (ROI). It is a post-processing method applied to data collected by Full Matrix Capture (FMC) acquisition [6], which involves

* Corresponding author. CEA List, Centre de Saclay, Bâtiment Digiteo 565, 91191 Gif-sur-Yvette, France.
E-mail address: ksy@eddyfi.com (K. Sy).

a succession of ultrasonic shots from the elements of the array. For each such shot, a transmitter emits a wave which is received by all elements of the transducer after propagation within the medium. After digitization of the signal, we obtain the matrix of acquisition, also named inter-element matrix, which is a 3D matrix of size $N \times N \times Q$, where N is the number of elements of the sensor and Q is the number of time samples.

In the ROI, we compute from each couple of elements the time of flight required to travel between the transmitting element via the focusing point to the receiving element. At this time of flight is associated an amplitude from the signal of the inter-element matrix. The different contributions coming from the different elementary signals constructively sum up when a reflector is present, and cancel out otherwise.

Let K be the inter-element matrix acquired by FMC, the TFM amplitude $I^m(P)$, for a given mode of reconstruction m, at the focusing point P, is given by the relation (1)

$$I^m(P) = \sum_{i=1}^{N} \sum_{j=1}^{N} K_{ij}(t_{ij}^m(P)), \tag{1}$$

where $t_{ij}^m(P)$ is the time of flight necessary to follow the path between the transmitter i and the receiver j via the focusing point P, for a mode m. The reconstruction mode m is defined by the ultrasonic path used for the time of flight calculation.

2.1. Ultrasonic paths

The waves refracted in the specimen can propagate along different paths according to their refraction angle. These waves (longitudinal or transverse) can be converted at interfaces of the piece or when interacting with a defect. When the path between the elements and the running point P is without reflection on the backwall (Fig. 1), the mode is called direct mode. The combination of longitudinal (L) and transverse (T) waves leads to four reconstruction modes. LL (or TT) designates the mode for which the return trip is with longitudinal wave (or transverse wave) while LT and TT designate the modes with conversion on the defect.

Following the same principle, corner echo modes (Fig. 2), also called half skip modes, include reflection on the backwall before interaction with the defect. The combination of longitudinal and transverse waves yields eight reconstruction modes (LLL, LLT, LTL, TLL, LTT, TLT, TTL, TTT).

Indirect modes, denoted also full skip modes (Fig. 3), include two reflection on the back wall, one after emission and one before the reception of the wave. It leads to sixteen indirect modes (LLLL, LLLT, LLTL …).

With the same reasoning, it is possible to take into account a large number of paths, generating as many reconstruction modes. Depending upon the selected path, in the case of crack-type defects, the signature of the specular echo along the defect and the one of the diffraction by the edges are additional information for the characterization of the defects.

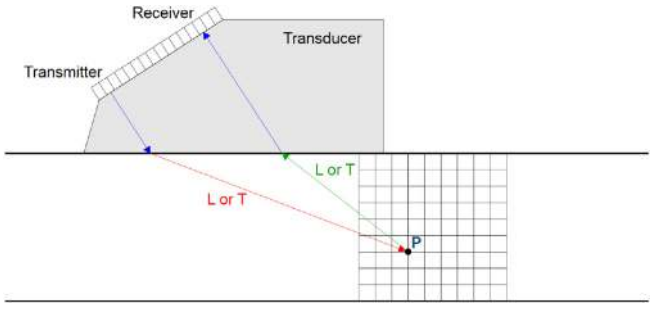

Fig. 1. Example of ultrasonic paths of the waves emitted by the array: direct mode.

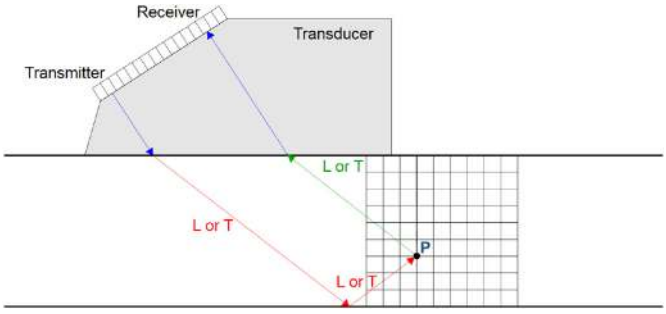

Fig. 2. Example of ultrasonic paths of the waves emitted by the array: corner echo mode.

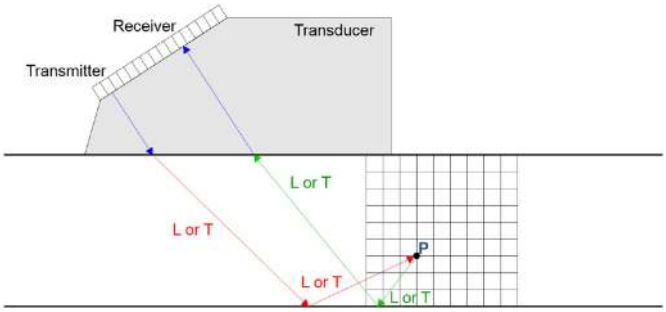

Fig. 3. Example of ultrasonic paths of the waves emitted by the array: indirect mode.

2.2. Diffraction echoes in TFM imaging

The conventional TFM (direct mode LL, TT) applied to crack, generally allows to find the signature of the diffraction [7] by the defect tips, which is relevant for the defect sizing.

The multidirectional behaviour of diffraction is a true advantage since it is little sensitive to defect orientation. However, diffraction energy is generally low and can be quickly embedded in noise or strongly attenuated in some materials. In addition, crack diffraction echoes are very similar to volumetric defects echoes, making it not easy to distinguish these two kinds of defect. One way to distinguish them is to exploit specular echoes which, when they exist, provide very different TFM images of both types of defects.

2.3. Specular echoes in TFM imaging

Specular echoes have the main advantage of being very energetic compared with diffraction echoes, but incident waves are reflected into a preferential direction according to the Snell-Descartes law, which depends on reflector orientation. Thus, during the TFM reconstruction, this is not all paths which respect this law. But if relevant paths are used, specular echoes, contained in the temporal signal, are spatially repositioned along the defect. This signature will make it possible to conclude upon the surface nature of the planar defect unambiguously.

2.4. TFM multi-modes

Several works [3–5,8,9] have shown the potential of multi-modes TFM imaging, particularly corner echo modes, for migrating specular echoes in the case of defects which interest us.

To illustrate the behaviour of multi-modes TFM imaging, the algorithm has been applied on experimental data, acquired for the inspection configuration in Fig. 4. The defect to be detected, 10 mm high, are inner surface-breaking notches which are generated artificially by electro-erosion, in ferritic steel piece.

The experimental acquisitions are obtained by an Imasonic array

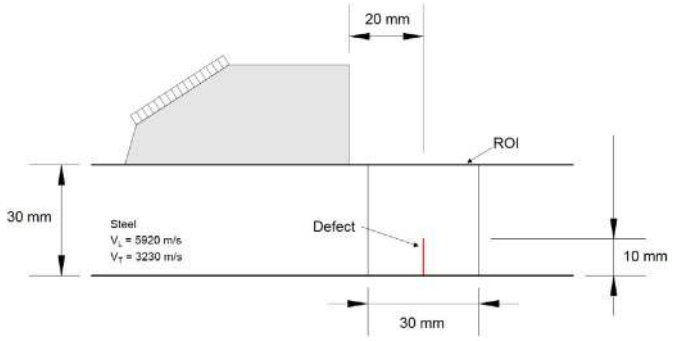

Fig. 4. Inspection configuration. The sides of the part are parallel. The probe has 64 elements and its central frequency is equal to 5 MHz.

Table 1
Transducer characteristics.

Characteristics	Value
Number of elements	64
Pitch	0.6 mm
element length	0.5 mm
Central frequency	5 MHz
Refraction angle of transverse waves	55

[13], of which characteristics are in Table 1, controlled by a Multi X system [14].

The TFM imaging is carried out in the ROI defined in Fig. 4.

The direct mode TT and all corner echo modes are calculated (Fig. 5). Each image is normalized with respect to the maximal amplitude of the TT mode which contains the most energetic pixel (Fig. 6).

In this configuration, only the TTT mode allows the defect profile to be reconstructed by specular echoes. Direct mode TT brings diffraction as well as, with smaller amplitude, TLT, LLT and TTL modes. All others bring echoes not re-positioned at the defect position, which are called artefacts.

To avoid many TFM calculations and images analysis which can be tedious and can suffer from the misinterpretation due to the presence of artefacts, it is necessary to a priori know the relevant modes for the defect to be detected in order to reliably reconstruct it. It is within this context that a method of predicting the modes relevant to surface defects is proposed thereafter.

3. Prediction of relevant modes

To predict the relevant modes, the Specular Echoes Estimator (SEE) has been developed. SEE is a tool that predicts the sensitivity of a given mode for a planar defect whose orientation is known whatever its position and height. It provides a mapping of detectability for which the larger the amplitude, the better the defect detection.

3.1. The specular echoes estimator

The algorithm is based on the calculation of the elastic field reflected by a surface defect of normal $\mathbf{n}$. The hypothesis of the knowledge of defect orientation is thus made. The latter is generally known when stresses applied to the inspected area are known.

The calculation starts from considering that at each point of the ROI, there exists a defect, passing through this point. For each couple of elements, the specular echo from the running point is thus calculated. To model the beam-defect interaction, a specular model is developed. Under the assumption that the computation point is located in the far field, waves can be approximated by plane waves. So, for a point of observation P belonging to a defect of normal $\mathbf{n}$, the displacement vector of the wave transmitted by the element i and received by the element j, at this point, is given by

$$\mathbf{u_{ij}}(P,\, t = t_{ij}^P) = A_{ij}(P,\, \mathbf{n})\delta(t - t_{ij}^P)\mathbf{p}, \tag{2}$$

where $A_{ij}(P, \mathbf{n})$ is the wave amplitude, $t_{ij}^P = t_i^P + t_j^P$ is the sum of the times of flight between transmitter i and P, t_i^P, and the one between receiver j and P, t_j^P, and $\mathbf{p}$ the polarisation vector.

The displacement amplitude can be decomposed [10] as follows:

$$A_{ij}(P,\mathbf{n}) = \begin{cases} A_i(P)A_j(P)R_{ij}(P,\mathbf{n}) & \text{if the path } i \to P \to j \text{ is specular,} \\ 0 & \textit{otherwise,} \end{cases} \tag{3}$$

where $R_{ij}(P, \mathbf{n})$ is the reflection coefficient on the defect at the point P, $A_i(P)$ the amplitude of the wave emitted by the element i at point P and $A_j(P)$ the one emitted by the element j at the same point P.

The defect being considered as a perfect reflector, the reflection coefficients are calculated for a solid/empty interface.

Relation (3) shows that the amplitude is non zero if Snell's law is respected at the running point. To check this law, one compares a so-called theoretical normal and the normal of the defect to be detected. One defines this theoretical normal for the considered path as the vector resulting from the summation of the incident and reflected slowness vectors. The slowness vector is the vector along the direction of propagation of the wave and of amplitude equal to the inverse of its phase velocity in this direction.

Let $\mathbf{s_i^P}$ and $\mathbf{s_j^P}$ be the incident and reflected slowness vectors at point P. For simplicity, indices ^{P} will no longer be indicated. The theoretical normal $\mathbf{n_{ij}}$ follows from

$$\mathbf{n_{ij}} = \frac{\mathbf{s_i} + \mathbf{s_j}}{\|\mathbf{s_i} + \mathbf{s_j}\|}. \tag{4}$$

The path is specular if

$$|\mathbf{n}.\, \mathbf{n_{ij}}| = 1 \tag{5}$$

So equation (3) becomes:

$$A_{ij}(P,\mathbf{n}) = \begin{cases} A_i(P)A_j(P)R_{ij}(P,\mathbf{n}) \text{ if } |\mathbf{n}.\mathbf{n_{ij}}|=1, \\ 0 \text{ otherwise.} \end{cases} \tag{6}$$

At each point, in accordance with the FMC acquisition, the amplitude associated to it is the summation of the amplitudes of all couples of transmitter-receiver, so the total contribution of a point P belonging to a defect with normal $\mathbf{n}$ for an array made of N elements is

$$A(P,\, \mathbf{n}) = \sum_{i=1}^{N}\sum_{j=1}^{N} \begin{cases} A_i(P)A_j(P)R_{ij}(P,\, \mathbf{n}) \textit{ if } |\mathbf{n}.\, \mathbf{n_{ij}}| = 1, \\ 0 \textit{ otherwise.} \end{cases} \tag{7}$$

From this relation, we construct the SEE mapping for a defined ROI. The larger the amplitude of the mapping, the better the detection. A null corresponds with an impossible reconstruction of the defect by specular echoes.

3.2. SEE mapping

To illustrate the developed model, one computes, from the previous configuration (Fig. 4), the SEE mapping for a 0° orientated defect with respect to the vertical, following the TTT mode.

The field amplitude is obtained by through the use of the CIVA software [12] which tackles the elastodynamic equations by the pencil model [11].

Furthermore, the probability to verify the equality $|\mathbf{n}.\, \mathbf{n_{ij}}| = 1$ is null in discrete calculations, so we use a tolerance such as $|\mathbf{n}.\, \mathbf{n_{ij}}| > 0.99$.

The SEE mapping (Fig. 7) predicts that a vertical defect, located at the upper part of the piece, will not be reconstructed following TTT mode.

A defect located in the bottom part will be reconstructed. The SNR will be maximised if the defect is in the blue area corresponding to a maximal amplitude.

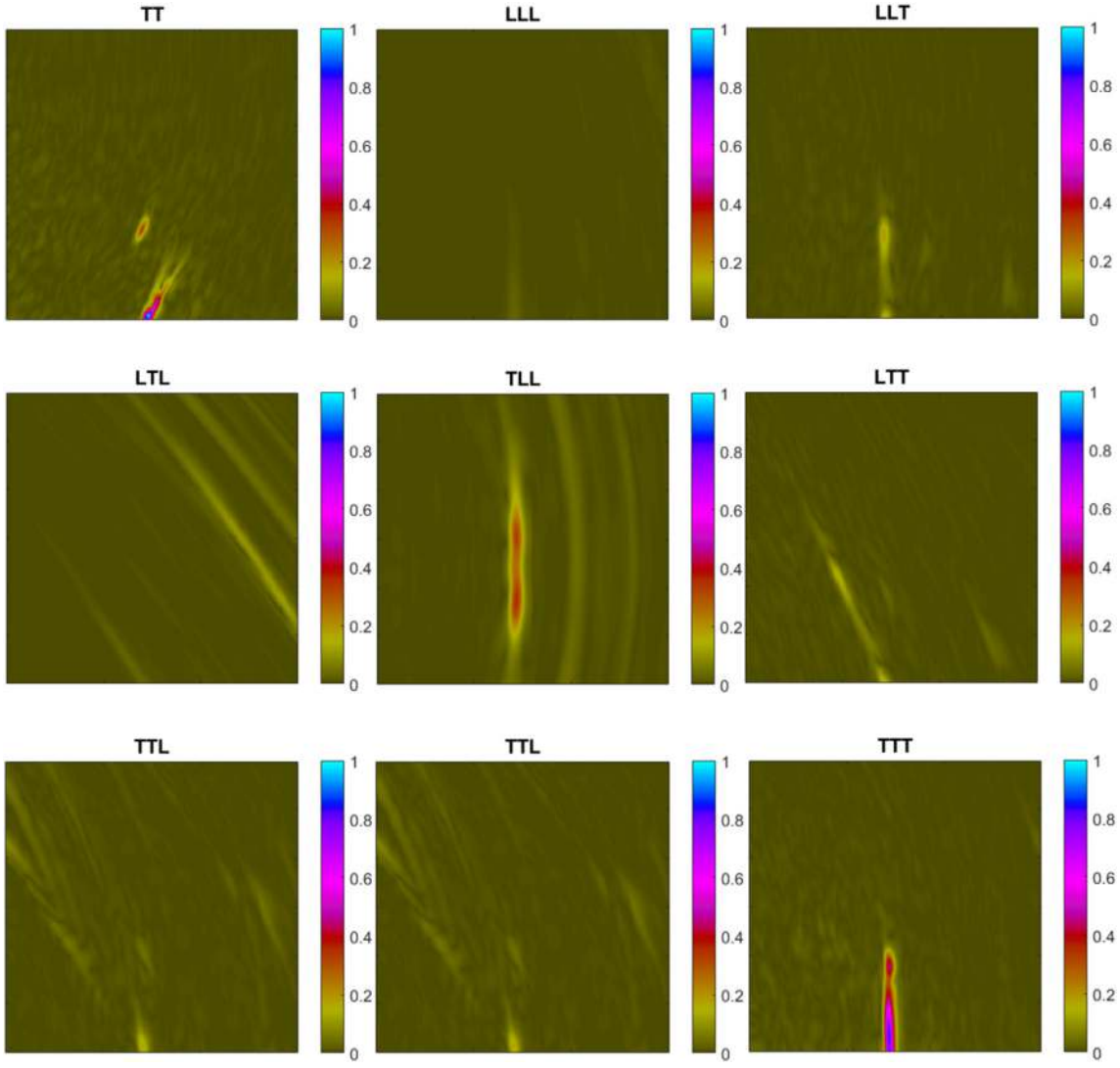

Fig. 5. TFM images.

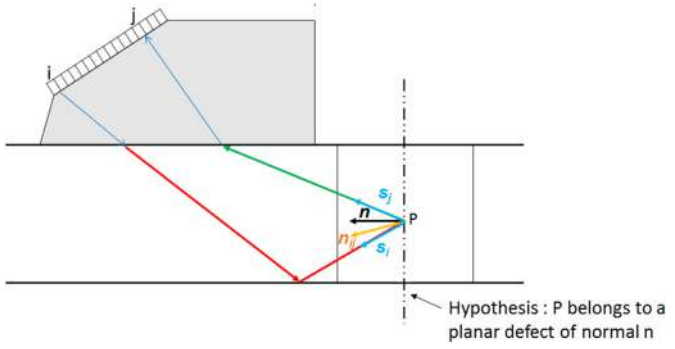

Fig. 6. Determination of the theoretical vector from slowness vectors at focusing point *P*. This calculation is performed at all points of the ROI and for all pairs of elements.

To validate this prediction, we are going to compare SEE mappings and defect TFM images.

4. Exploitation of SEE mappings and comparison with TFM images

To show the relevance of the specular echoes estimator tool, we completed FMC acquisitions in two specimens presenting vertical defects. Defects, 10 mm high, are inner surface-breaking notches.

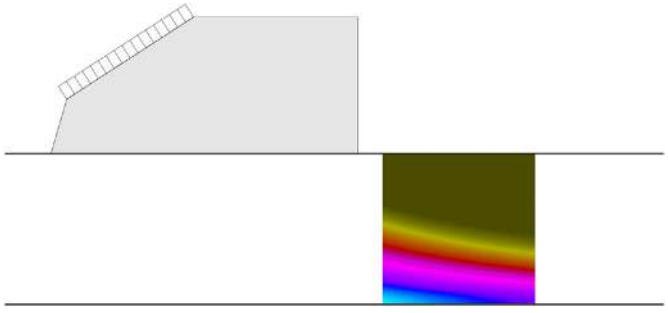

Fig. 7. TTT SEE mapping for a planar defect orientated at 0°.

Both configurations have been reproduced by simulation. We calculate the SEE mappings and the associated TFM images on the simulated and experimental data for different modes.

4.1. First case

Configuration is that considered in Fig. 4.

For the three TTL, TLT and TTT corner echo modes, chosen arbitrarily, the SEE mappings for a planar defect orientated at 0° as well as

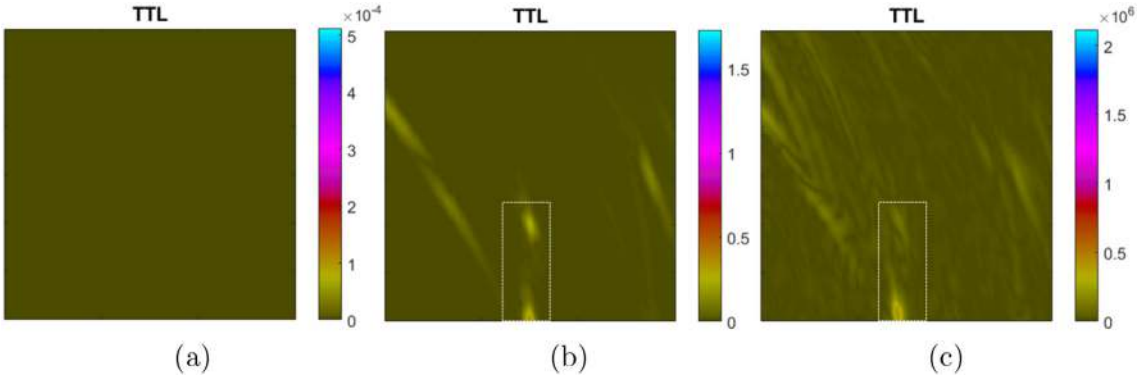

Fig. 8. (a) SEE mapping, (b) TFM image on simulated data, (c) TFM image on experimental data for TTL mode.

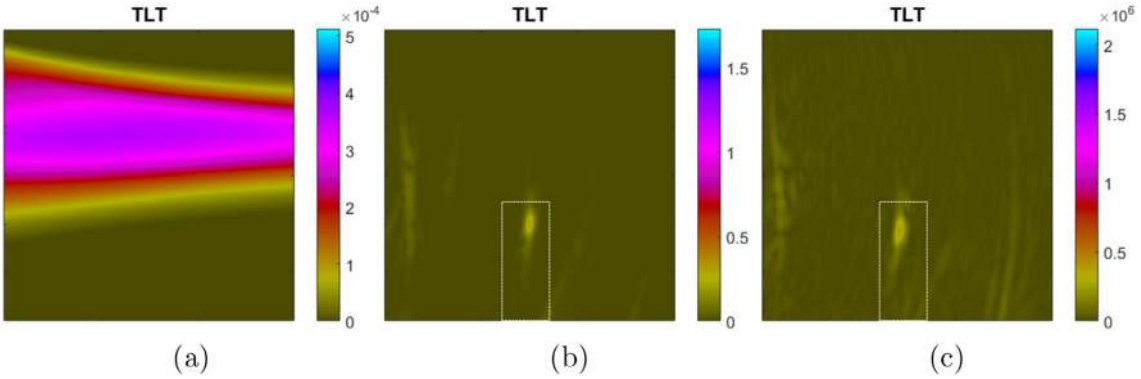

Fig. 9. (a) SEE mapping, (b) TFM image on simulated data, (c) TFM image on experimental data for TLT mode.

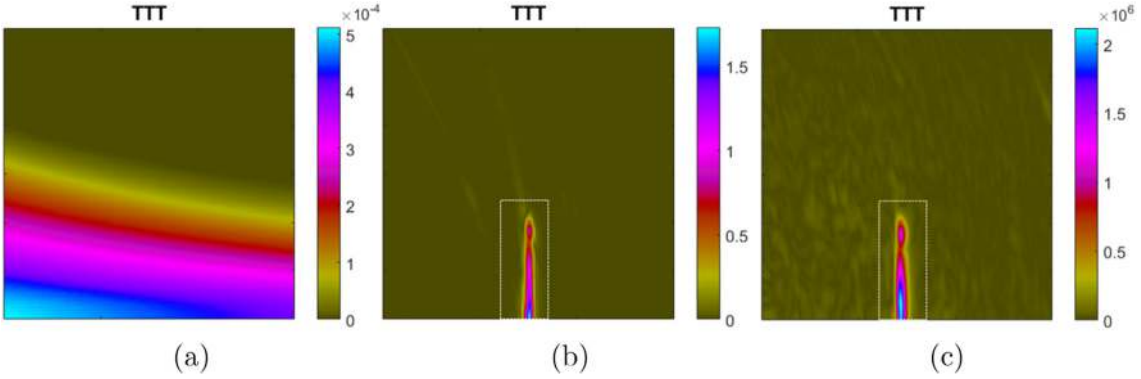

Fig. 10. (a) SEE mapping for vertical defect, (b) TFM image on simulated data, (c) TFM image on experimental data for TTT mode.

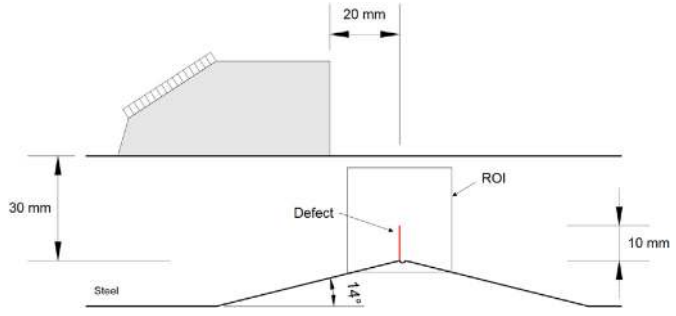

Fig. 11. Inspection configuration: The angle of inclination of the bottom is 14°.

the TFM reconstructions of the associated simulated and experimental data have been computed.

TTL mode (Fig. 8) shows a null SEE mapping at any point in the ROI. The associated TFM images show perfect consistency with it, the defects are not retrieved by specular echoes. Diffraction echoes may appear, as in this case, because SEE just predicts detectability of specular echoes.

For the TLT mode (Fig. 9), the SEE mapping shows that only a defect in the upper half of the piece can be reconstructed. An inner surface-breaking defect is therefore not detectable by this mode, as seen in the simulated and experimental TFM images.

TTT mode (Fig. 10) is the only one to enable the reconstruction of the defect both from the simulated and experimental data in accordance with its SEE mapping, which shows energy in the lower half of the ROI where the defect is located. Another important remark is that the variation of amplitude along the defect is qualitatively the same variation as the one observed in the SEE mapping.

All above results confirm that the TFM reconstruction is coherent with the SEE mapping. So, the same comparisons have been carried out for the second piece.

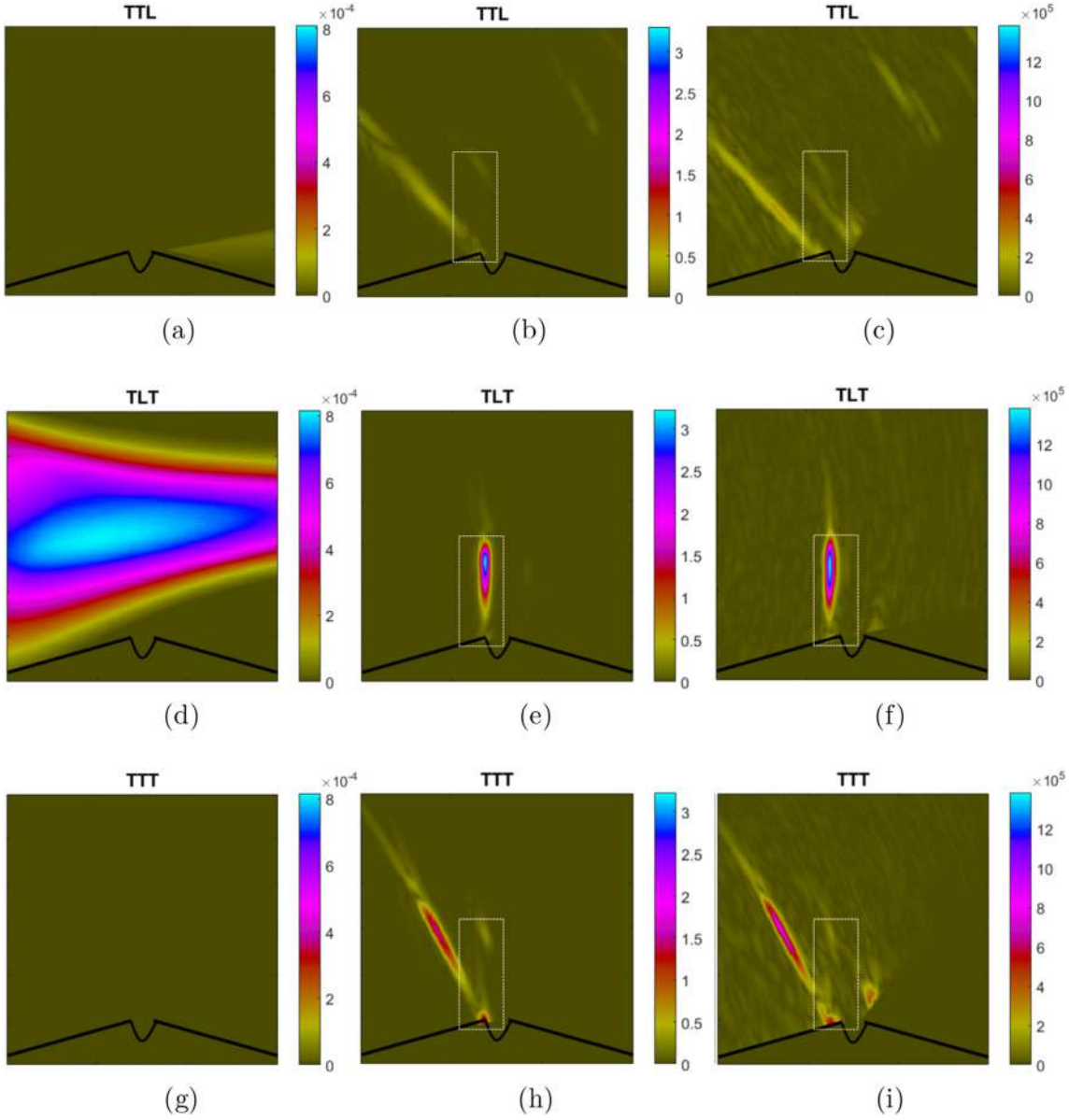

Fig. 12. Validation of the SEE mapping for the TTL, TLT and TTT modes for a piece with a slope of 14°. (a,d,g) SEE mappings, (b,e,h) TFM on simulated data, (c, f, i)TFM on experimental data. The black line corresponds to the back wall (Case 2).

4.2. Second case

In the second example proposed, only the geometry of the piece is different to the previous configuration as illustrated in Fig. 11.

TFM images and SEE mapping are calculated for the three modes TTL, TLT and TTT.

For this piece (Fig. 12), the TLT SEE mapping shows that for an inner surface-breaking defect, the lower part will not be detected, in agreement with simulated and experimental TFM images. Note that the partial reconstruction of the defect is due to the choice of the TLT mode and not to the geometry of the defect.

The TTL and TTT modes are not pertinent for a vertically-orientated defect, their map is equal to zero at all points, and as predicted, TTL and TTT TFM images do not enable the defect to be imaged. SEE mapping allows also to predict that the only present echo is an artefact.

5. Conclusion

TFM imaging produces realistic representations of defects from diffraction phenomena and specular reflections. In particular, specular echoes are an asset for characterizing strong defects, but they remain very sensitive to their orientations. To overcome this limitation, it is feasible to use multi-mode TFM imaging which allows consideration of a large number of ultrasonic paths, thus increasing the possibility of obtaining a specular path. However, applying the TFM algorithm for a large number of modes is tedious and might even be counter-productive due to artefacts that are possibly appearing.

It is within this context that the Specular Echoes Estimator (SEE) has been developed to predict the detectability of a planar defect the orientation of which is known. It is based on a model of beam-defect interaction which only takes into account the specular phenomenon. The mapping produced shows the area where a defect can be imaged or not. So, the SEE mapping predicts the defect reconstruction whatever its location and its height. In addition, all modes presenting a null mapping are automatically discarded, removing the need to reconstruct defects with modes which are not relevant and could be a source of artefact formation.

Several validations have been run on simulated and experimental

data and show a good accordance between SEE mappings and TFM images. Whenever the SEE mappings predict the detectability of defects, these defects are well reconstructed and vice-versa. SEE appears as very helpful for TFM imaging, allowing the prediction of the relevant modes.

Additionally, it has been shown that the variation of the TFM amplitude on a defect is close to the variation of SEE mapping at the same position. This characteristic could be exploited for defect sizing. The SEE estimator could also help to define the best relative position of the probe with respect to the defect and even the best probe to use for an optimal detection by comparing SEE mappings of different probes.

References

[1] Karaman M, Pai-Chi L, O'Donnell M. Synthetic aperture imaging for small scale systems. IEEE Trans Ultrason Ferroelectrics Freq Contr 1995;42(3):429–42.

[2] Holmes C, Drinkwater BW, Wilcox PD. Post-processing of the full matrix of ultrasonic transmit-receive array data for non-destructive evaluation. NDT E Int 2005;38(8):701–11.

[3] Zhang J, Drinkwater BW, Wilcox PD, Hunter AJ. Defect detection using ultrasonic arrays: the multi-mode total focusing method. NDT E Int 2010;43(2):123–33.

[4] Fidahoussen A, Calmon P, Lambert M, Chatillon S. Imaging of defects in several complex configurations by simulation-helped processing of ultrasonic array data, review of progress in quantitative nondestructive evaluation, 847854. 2010. https://doi.org/10.1063/1.3362502.

[5] Le Jeune L, Robert S, Lopez Villaverde E, Prada C. Plane wave imaging for ultrasonic non-destructive testing: generalization to multimodal imaging. Ultrasonics 2016;64:128–38.

[6] Sutcliffe M, Weston M, Dutton B, Charlton P, Donne K. Real-time full matrix capture for ultrasonic non-destructive testing with acceleration of post-processing through graphic hardware. NDT E Int 2012;51(10):16–23.

[7] Ogilvy JA, Temple JAG. Diffraction of elastic waves by cracks: application to time-of-flight inspection: application to ultrasonic field computation. Ultrasonics 1983;21(6):259–69.

[8] Iakovleva E, Chatillon S, Bredif P, Mahaut S. Multi-mode TFM imaging with artifacts filtering using CIVA UT forwards models. AIP Conf. Proc. 2014;1581(1):72.

[9] Han XL, Wu WT, Li P, Temple JL. Combination of direct, half-skip and full-skip TFM to characterize multi-faceted crack, 2015. Taipei: IEEE International Ultrasonics Symposium; 2015. p. 1–4. https://doi.org/10.1109/ULTSYM.2015.0339.

[10] Brekhovskikh M. Waves in layered media. New York: Academic Press; 1960.

[11] Gengembre N, Lhémery A. Pencil method in elastodynamics: application to ultrasonic field computation. Ultrasonics 2000;31(1–8):495–9.

[12] CIVA software website, http://www-civa.cea.fr.

[13] http://www.imasonic.com/Company/IdentityF.php.

[14] http://www.m2m-ndt.com/.